

Fermi National Accelerator Laboratory

FERMILAB-Pub-98/133-E

CDF

**Measurement of the $\sigma(W+ \geq 1 \text{ Jet})/\sigma(W)$ Cross Section Ratio from $\bar{p}p$
Collisions at $\sqrt{s} = 1.8 \text{ TeV}$**

F. Abe et al.

The CDF Collaboration

*Fermi National Accelerator Laboratory
P.O. Box 500, Batavia, Illinois 60510*

April 1998

Submitted to *Physical Review Letters*

Disclaimer

This report was prepared as an account of work sponsored by an agency of the United States Government. Neither the United States Government nor any agency thereof, nor any of their employees, makes any warranty, expressed or implied, or assumes any legal liability or responsibility for the accuracy, completeness, or usefulness of any information, apparatus, product, or process disclosed, or represents that its use would not infringe privately owned rights. Reference herein to any specific commercial product, process, or service by trade name, trademark, manufacturer, or otherwise, does not necessarily constitute or imply its endorsement, recommendation, or favoring by the United States Government or any agency thereof. The views and opinions of authors expressed herein do not necessarily state or reflect those of the United States Government or any agency thereof.

Distribution

Approved for public release; further dissemination unlimited.

**Measurement of the $\sigma(W + \geq 1 \text{ Jet})/\sigma(W)$ Cross Section Ratio
from $\bar{p}p$ Collisions at $\sqrt{s} = 1.8 \text{ TeV}$**

F. Abe,¹⁷ H. Akimoto,³⁹ A. Akopian,³¹ M. G. Albrow,⁷ A. Amadon,⁵ S. R. Amendolia,²⁷ D. Amidei,²⁰ J. Antos,³³
 S. Aota,³⁷ G. Apollinari,³¹ T. Arisawa,³⁹ T. Asakawa,³⁷ W. Ashmanskas,¹⁸ M. Atac,⁷ P. Azzi-Bacchetta,²⁵
 N. Bacchetta,²⁵ S. Bagdasarov,³¹ M. W. Bailey,²² P. de Barbaro,³⁰ A. Barbaro-Galtieri,¹⁸ V. E. Barnes,²⁹
 B. A. Barnett,¹⁵ M. Barone,⁹ G. Bauer,¹⁹ T. Baumann,¹¹ F. Bedeschi,²⁷ S. Behrends,³ S. Belforte,²⁷ G. Bellettini,²⁷
 J. Bellinger,⁴⁰ D. Benjamin,³⁵ J. Bensinger,³ A. Beretvas,⁷ J. P. Berge,⁷ J. Berryhill,⁵ S. Bertolucci,⁹ S. Bettelli,²⁷
 B. Bevensee,²⁶ A. Bhatti,³¹ K. Biery,⁷ C. Bigongiari,²⁷ M. Binkley,⁷ D. Bisello,²⁵ R. E. Blair,¹ C. Blocker,³
 S. Blusk,³⁰ A. Bodek,³⁰ W. Bokhari,²⁶ G. Bolla,²⁹ Y. Bonushkin,⁴ D. Bortoletto,²⁹ J. Boudreau,²⁸ L. Breccia,²
 C. Bromberg,²¹ N. Bruner,²² R. Brunetti,² E. Buckley-Geer,⁷ H. S. Budd,³⁰ K. Burkett,²⁰ G. Busetto,²⁵
 A. Byon-Wagner,⁷ K. L. Byrum,¹ M. Campbell,²⁰ A. Caner,²⁷ W. Carithers,¹⁸ D. Carlsmith,⁴⁰ J. Cassada,³⁰
 A. Castro,²⁵ D. Cauz,³⁶ A. Cerri,²⁷ P. S. Chang,³³ P. T. Chang,³³ H. Y. Chao,³³ J. Chapman,²⁰ M. -T. Cheng,³³
 M. Chertok,³⁴ G. Chiarelli,²⁷ C. N. Chiou,³³ F. Chlebana,⁷ L. Christofek,¹³ M. L. Chu,³³ S. Cihangir,⁷
 A. G. Clark,¹⁰ M. Cobal,²⁷ E. Cocca,²⁷ M. Contreras,⁵ J. Conway,³² J. Cooper,⁷ M. Cordelli,⁹ D. Costanzo,²⁷
 C. Couyoumtzelis,¹⁰ D. Cronin-Hennessy,⁶ R. Culbertson,⁵ D. Dagenhart,³⁸ T. Daniels,¹⁹ F. DeJongh,⁷
 S. Dell'Agnello,⁹ M. Dell'Orso,²⁷ R. Demina,⁷ L. Demortier,³¹ M. Deninno,² P. F. Derwent,⁷ T. Devlin,³²
 J. R. Dittmann,⁶ S. Donati,²⁷ J. Done,³⁴ T. Dorigo,²⁵ N. Eddy,²⁰ K. Einsweiler,¹⁸ J. E. Elias,⁷ R. Ely,¹⁸
 E. Engels, Jr.,²⁸ W. Erdmann,⁷ D. Errede,¹³ S. Errede,¹³ Q. Fan,³⁰ R. G. Feild,⁴¹ Z. Feng,¹⁵ C. Ferretti,²⁷ I. Fiori,²
 B. Flaughner,⁷ G. W. Foster,⁷ M. Franklin,¹¹ J. Freeman,⁷ J. Friedman,¹⁹ H. Frisch,⁵ Y. Fukui,¹⁷ S. Gadomski,¹⁴
 S. Galeotti,²⁷ M. Gallinaro,²⁶ O. Ganel,³⁵ M. Garcia-Sciveres,¹⁸ A. F. Garfinkel,²⁹ C. Gay,⁴¹ S. Geer,⁷
 D. W. Gerdes,¹⁵ P. Giannetti,²⁷ N. Giokaris,³¹ P. Giromini,⁹ G. Giusti,²⁷ M. Gold,²² A. Gordon,¹¹ A. T. Goshaw,⁶
 Y. Gotra,²⁸ K. Goulianos,³¹ H. Grassmann,³⁶ L. Groer,³² C. Grosso-Pilcher,⁵ G. Guillian,²⁰ J. Guimaraes da
 Costa,¹⁵ R. S. Guo,³³ C. Haber,¹⁸ E. Hafen,¹⁹ S. R. Hahn,⁷ R. Hamilton,¹¹ T. Handa,¹² R. Handler,⁴⁰
 F. Happacher,⁹ K. Hara,³⁷ A. D. Hardman,²⁹ R. M. Harris,⁷ F. Hartmann,¹⁶ J. Hauser,⁴ E. Hayashi,³⁷ J. Heinrich,²⁶
 W. Hao,³⁵ B. Hinrichsen,¹⁴ K. D. Hoffman,²⁹ M. Hohlmann,⁵ C. Holck,²⁶ R. Hollebeek,²⁶ L. Holloway,¹³ Z. Huang,²⁰
 B. T. Huffman,²⁸ R. Hughes,²³ J. Huston,²¹ J. Huth,¹¹ H. Ikeda,³⁷ M. Incagli,²⁷ J. Incandela,⁷ G. Introzzi,²⁷
 J. Iwai,³⁹ Y. Iwata,¹² E. James,²⁰ H. Jensen,⁷ U. Joshi,⁷ E. Kajfasz,²⁵ H. Kambara,¹⁰ T. Kamon,³⁴ T. Kaneko,³⁷
 K. Karr,³⁸ H. Kasha,⁴¹ Y. Kato,²⁴ T. A. Keaffaber,²⁹ K. Kelley,¹⁹ R. D. Kennedy,⁷ R. Kephart,⁷ D. Kestenbaum,¹¹
 D. Khazins,⁶ T. Kikuchi,³⁷ B. J. Kim,²⁷ H. S. Kim,¹⁴ S. H. Kim,³⁷ Y. K. Kim,¹⁸ L. Kirsch,³ S. Klimenko,⁸
 D. Knoblauch,¹⁶ P. Koehn,²³ A. Königeter,¹⁶ K. Kondo,³⁷ J. Konigsberg,⁸ K. Kordas,¹⁴ A. Korytov,⁸ E. Kovacs,¹
 W. Kowald,⁶ J. Kroll,²⁶ M. Kruse,³⁰ S. E. Kuhlmann,¹ E. Kuns,³² K. Kurino,¹² T. Kuwabara,³⁷ A. T. Laasanen,²⁹
 S. Lami,²⁷ S. Lammel,⁷ J. I. Lamoureux,³ M. Lancaster,¹⁸ M. Lanzoni,²⁷ G. Latino,²⁷ T. LeCompte,¹ S. Leone,²⁷
 J. D. Lewis,⁷ P. Limon,⁷ M. Lindgren,⁴ T. M. Liss,¹³ J. B. Liu,³⁰ Y. C. Liu,³³ N. Lockyer,²⁶ O. Long,²⁶
 C. Loomis,³² M. Loretì,²⁵ D. Lucchesi,²⁷ P. Lukens,⁷ S. Lusin,⁴⁰ J. Lys,¹⁸ K. Maeshima,⁷ P. Maksimovic,¹¹
 M. Mangano,²⁷ M. Mariotti,²⁵ J. P. Marriner,⁷ A. Martin,⁴¹ J. A. J. Matthews,²² P. Mazzanti,² P. McIntyre,³⁴
 P. Melese,³¹ M. Menguzzato,²⁵ A. Menzione,²⁷ E. Meschi,²⁷ S. Metzler,²⁶ C. Miao,²⁰ T. Miao,²² G. Michail,¹¹
 R. Miller,²¹ H. Minato,³⁷ S. Miscetti,⁹ M. Mishina,¹⁷ S. Miyashita,³⁷ N. Moggi,²⁷ E. Moore,²² Y. Morita,¹⁷
 A. Mukherjee,⁷ T. Muller,¹⁶ P. Murat,²⁷ S. Murgia,²¹ M. Musy,³⁶ H. Nakada,³⁷ I. Nakano,¹² C. Nelson,⁷
 D. Neuberger,¹⁶ C. Newman-Holmes,⁷ C.-Y. P. Ngan,¹⁹ L. Nodulman,¹ A. Nomerotski,⁸ S. H. Oh,⁶ T. Ohmoto,¹²
 T. Ohsugi,¹² R. Oishi,³⁷ M. Okabe,³⁷ T. Okusawa,²⁴ J. Olsen,⁴⁰ C. Pagliarone,²⁷ R. Paoletti,²⁷ V. Papadimitriou,³⁵
 S. P. Pappas,⁴¹ N. Parashar,²⁷ A. Parri,⁹ J. Patrick,⁷ G. Pauletta,³⁶ M. Paulini,¹⁸ A. Perazzo,²⁷ L. Pescara,²⁵
 M. D. Peters,¹⁸ T. J. Phillips,⁶ G. Piacentino,²⁷ M. Pillai,³⁰ K. T. Pitts,⁷ R. Plunkett,⁷ A. Pompos,²⁹ L. Pondrom,⁴⁰
 J. Proudfoot,¹ F. Ptohos,¹¹ G. Punzi,²⁷ K. Ragan,¹⁴ D. Reher,¹⁸ M. Reischl,¹⁶ A. Ribon,²⁵ F. Rimondi,²
 L. Ristori,²⁷ W. J. Robertson,⁶ T. Rodrigo,²⁷ S. Rolli,³⁸ L. Rosenson,¹⁹ R. Roser,¹³ T. Saab,¹⁴ W. K. Sakumoto,³⁰
 D. Saltzberg,⁴ A. Sansoni,⁹ L. Santi,³⁶ H. Sato,³⁷ P. Schlabach,⁷ E. E. Schmidt,⁷ M. P. Schmidt,⁴¹ A. Scott,⁴
 A. Scribano,²⁷ S. Segler,⁷ S. Seidel,²² Y. Seiya,³⁷ F. Semeria,² T. Shah,¹⁹ M. D. Shapiro,¹⁸ N. M. Shaw,²⁹
 P. F. Shepard,²⁸ T. Shibayama,³⁷ M. Shojima,³⁷ M. Shochet,⁵ J. Siegrist,¹⁸ A. Sill,³⁵ P. Sinervo,¹⁴ P. Singh,¹³
 K. Sliwa,³⁸ C. Smith,¹⁵ F. D. Snider,¹⁵ J. Spalding,⁷ T. Speer,¹⁰ P. Sphicas,¹⁹ F. Spinella,²⁷ M. Spiropulu,¹¹
 L. Spiegel,⁷ L. Stanco,²⁵ J. Steele,⁴⁰ A. Stefanini,²⁷ R. Ströhmer,^{7*} J. Strolgas,¹³ F. Strumia,¹⁰ D. Stuart,⁷
 K. Sumorok,¹⁹ J. Suzuki,³⁷ T. Suzuki,³⁷ T. Takahashi,²⁴ T. Takano,²⁴ R. Takashima,¹² K. Takikawa,³⁷ M. Tanaka,³⁷
 B. Tannenbaum,²² F. Tartarelli,²⁷ W. Taylor,¹⁴ M. Tecchio,²⁰ P. K. Teng,³³ Y. Teramoto,²⁴ K. Terashi,³⁷

S. Tether,¹⁹ D. Theriot,⁷ T. L. Thomas,²² R. Thurman-Keup,¹ M. Timko,³⁸ P. Tipton,³⁰ A. Titov,³¹ S. Tkaczyk,⁷ D. Toback,⁵ K. Tollefson,¹⁹ A. Tollestrup,⁷ H. Toyoda,²⁴ W. Trischuk,¹⁴ J. F. de Troconiz,¹¹ S. Truitt,²⁰ J. Tseng,¹⁹ N. Turini,²⁷ T. Uchida,³⁷ F. Ukegawa,²⁶ J. Valls,³² S. C. van den Brink,²⁸ S. Vejcik, III,²⁰ G. Velev,²⁷ R. Vidal,⁷ R. Vilar,^{7,*} D. Vucinic,¹⁹ R. G. Wagner,¹ R. L. Wagner,⁷ J. Wahl,⁵ N. B. Wallace,²⁷ A. M. Walsh,³² C. Wang,⁶ C. H. Wang,³³ M. J. Wang,³³ A. Warburton,¹⁴ T. Watanabe,³⁷ T. Watts,³² R. Webb,³⁴ C. Wei,⁶ H. Wenzel,¹⁶ W. C. Wester, III,⁷ A. B. Wicklund,¹ E. Wicklund,⁷ R. Wilkinson,²⁶ H. H. Williams,²⁶ P. Wilson,⁵ B. L. Winer,²³ D. Winn,²⁰ D. Wolinski,²⁰ J. Wolinski,²¹ S. Worm,²² X. Wu,¹⁰ J. Wyss,²⁷ A. Yagil,⁷ W. Yao,¹⁸ K. Yasuoka,³⁷ G. P. Yeh,⁷ P. Yeh,³³ J. Yoh,⁷ C. Yosef,²¹ T. Yoshida,²⁴ I. Yu,⁷ A. Zanetti,³⁶ F. Zetti,²⁷ and S. Zucchelli²

(CDF Collaboration)

¹ Argonne National Laboratory, Argonne, Illinois 60439

² Istituto Nazionale di Fisica Nucleare, University of Bologna, I-40127 Bologna, Italy

³ Brandeis University, Waltham, Massachusetts 02254

⁴ University of California at Los Angeles, Los Angeles, California 90024

⁵ University of Chicago, Chicago, Illinois 60637

⁶ Duke University, Durham, North Carolina 27708

⁷ Fermi National Accelerator Laboratory, Batavia, Illinois 60510

⁸ University of Florida, Gainesville, FL 32611

⁹ Laboratori Nazionali di Frascati, Istituto Nazionale di Fisica Nucleare, I-00044 Frascati, Italy

¹⁰ University of Geneva, CH-1211 Geneva 4, Switzerland

¹¹ Harvard University, Cambridge, Massachusetts 02138

¹² Hiroshima University, Higashi-Hiroshima 724, Japan

¹³ University of Illinois, Urbana, Illinois 61801

¹⁴ Institute of Particle Physics, McGill University, Montreal H3A 2T8, and University of Toronto, Toronto M5S 1A7, Canada

¹⁵ The Johns Hopkins University, Baltimore, Maryland 21218

¹⁶ Institut für Experimentelle Kernphysik, Universität Karlsruhe, 76128 Karlsruhe, Germany

¹⁷ National Laboratory for High Energy Physics (KEK), Tsukuba, Ibaraki 305, Japan

¹⁸ Ernest Orlando Lawrence Berkeley National Laboratory, Berkeley, California 94720

¹⁹ Massachusetts Institute of Technology, Cambridge, Massachusetts 02139

²⁰ University of Michigan, Ann Arbor, Michigan 48109

²¹ Michigan State University, East Lansing, Michigan 48824

²² University of New Mexico, Albuquerque, New Mexico 87131

²³ The Ohio State University, Columbus, OH 43210

²⁴ Osaka City University, Osaka 588, Japan

²⁵ Università di Padova, Istituto Nazionale di Fisica Nucleare, Sezione di Padova, I-35131 Padova, Italy

²⁶ University of Pennsylvania, Philadelphia, Pennsylvania 19104

²⁷ Istituto Nazionale di Fisica Nucleare, University and Scuola Normale Superiore of Pisa, I-56100 Pisa, Italy

²⁸ University of Pittsburgh, Pittsburgh, Pennsylvania 15260

²⁹ Purdue University, West Lafayette, Indiana 47907

³⁰ University of Rochester, Rochester, New York 14627

³¹ Rockefeller University, New York, New York 10021

³² Rutgers University, Piscataway, New Jersey 08855

³³ Academia Sinica, Taipei, Taiwan 11530, Republic of China

³⁴ Texas A&M University, College Station, Texas 77843

³⁵ Texas Tech University, Lubbock, Texas 79409

³⁶ Istituto Nazionale di Fisica Nucleare, University of Trieste/Udine, Italy

³⁷ University of Tsukuba, Tsukuba, Ibaraki 315, Japan

³⁸ Tufts University, Medford, Massachusetts 02155

³⁹ Waseda University, Tokyo 169, Japan

⁴⁰ University of Wisconsin, Madison, Wisconsin 53706

⁴¹ Yale University, New Haven, Connecticut 06520

(April 28, 1998)

The ratio of the $W + \geq 1$ jet cross section to the inclusive W cross section is measured using $W^\pm \rightarrow e^\pm \nu$ events from $\bar{p}p$ collisions at $\sqrt{s} = 1.8$ TeV. The data are from 108 pb^{-1} of integrated luminosity collected with the Collider Detector at Fermilab (CDF). Measurements of the cross section ratio for jet transverse energy thresholds (E_T^{min}) ranging from 15 to 95 GeV are compared to theoretical predictions using next-to-leading-order QCD calculations. Data and theory agree well for $E_T^{min} > 25$ GeV, where the predictions lie within 1 standard deviation of the measured values.

The measurement of jet properties in W boson events from $\bar{p}p$ collisions can be used to test perturbative quantum chromodynamics (QCD) at large momentum transfers. In previous studies by the CDF collaboration, jet production properties in W and Z boson events were compared to leading-order (LO) QCD predictions [1,2]. In this Letter, we test QCD predictions at next-to-leading order (NLO) by measuring the cross section ratio $\mathcal{R}_{10} = \sigma(W + \geq 1 \text{ jet})/\sigma(W)$. Measurements of $W + \text{jet}$ cross section ratios by the UA2 and UA1 collaborations agreed well with theoretical predictions and allowed measurements of the strong coupling constant α_s [3,4]. Recent measurements from the D0 collaboration, however, indicate a discrepancy between ratios of $W + \text{jet}$ cross sections and NLO QCD predictions [5,6].

We measure \mathcal{R}_{10} using 51437 $W^\pm \rightarrow e^\pm \nu$ candidates observed at the Collider Detector at Fermilab [7]. The principal detector elements used for this analysis are the central tracking chamber (CTC), vertex tracking chamber (VTX), and the calorimeters. The CTC is a cylindrical drift chamber that measures the momenta of charged particles in the pseudorapidity range $|\eta| < 1.1$ [8]. The VTX, a time-projection chamber, identifies interactions along the beam direction. Both tracking detectors are immersed in a 1.4 T solenoidal magnetic field. The electromagnetic and hadronic calorimeters, segmented in a projective tower geometry, cover the range $|\eta| < 4.2$ and measure the energies of electrons, photons, and jets.

The $W \rightarrow e\nu$ candidates are selected from events that pass a high transverse energy ($E_T = E \sin\theta$) electron trigger. The event selection requires an isolated electron [9] in the fiducial region of the central calorimeter ($|\eta| \leq 1.1$). The electron must have $E_T \geq 20$ GeV and satisfy tight selection criteria [10]. The reconstructed transverse energy of the neutrino, measured from the imbalance of E_T in the calorimeter (\cancel{E}_T) [11], must exceed 30 GeV. Jets in the W events are reconstructed by clustering energy depositions in the calorimeter using a cone algorithm [12] with radius $\Delta R \equiv \sqrt{(\Delta\eta)^2 + (\Delta\phi)^2} = 0.4$. This cone size was used for previous W and $Z + \text{jet}$ analyses [1,2]. The jet E_T is corrected for calorimeter response, underlying event energy within the jet cone, and energy contamination from additional $\bar{p}p$ interactions in the same bunch crossing [13]. Jets with $|\eta| \leq 2.4$ are selected for this analysis. To insure that jets are well separated from electrons, an event is rejected if any jet with $E_T \geq 12$ GeV lies within $\Delta R = 0.52$ of an electron.

We obtain \mathcal{R}_{10} by dividing the $W + \geq 1$ jet cross section for a particular minimum jet E_T threshold (E_T^{min}) by the inclusive W cross section. The cross section ratio measurement is corrected for backgrounds, acceptances, and efficiencies. Measuring a ratio of cross sections takes advantage of the cancellation of the integrated luminosity, and many systematic uncertainties are reduced. In this analysis, we measure \mathcal{R}_{10} for values of E_T^{min} that range from 15 to 95 GeV in 5 GeV increments. Of 51437

$W \rightarrow e\nu$ candidates, 7905 events have ≥ 1 jet with $E_T > 15$ GeV, and 214 events have ≥ 1 jet with $E_T > 95$ GeV.

The sources of background in the $W + \geq 1$ jet sample are summarized in Table I for $E_T^{min} = 15, 55,$ and 95 GeV. The largest background to $W \rightarrow e\nu$ production arises from QCD multijet production. In some multijet events, a jet is incorrectly reconstructed as an electron and a large \cancel{E}_T results from shower fluctuations or uninstrumented regions in the calorimeter. We measure this multijet contamination using an event sample obtained by removing the electron isolation and \cancel{E}_T requirements of the W selection [11]. The backgrounds also include several electroweak processes that yield an electron and \cancel{E}_T in the final state. We calculate backgrounds from $W \rightarrow \tau\nu$ (with $\tau \rightarrow e\nu\bar{\nu}$), $Z \rightarrow \tau^+\tau^-$, and $Z \rightarrow e^+e^-$ (where one electron is not identified) using the VECBOS Monte Carlo program [14] and a simulation of the CDF detector. The background calculation also removes a contribution from standard model $t\bar{t}$ production, in which one of the top quarks decays via $t \rightarrow Wb \rightarrow e\nu b$. In addition to these backgrounds, the number of ≥ 1 jet events is corrected to account for jets produced by additional $\bar{p}p$ interactions (“ X -jets”) and $W\gamma$ events in which the photon is reconstructed as a jet. The total $W + \geq 1$ jet background increases from $(22 \pm 5)\%$ at $E_T^{min} = 15$ GeV to $(44 \pm 13)\%$ at $E_T^{min} = 95$ GeV. The overall background to inclusive W events is $(5.9 \pm 1.2)\%$.

The acceptance for $W \rightarrow e\nu$ events, which corrects for losses due to the fiducial and kinematic requirements on the electron and \cancel{E}_T , is determined for each E_T^{min} using VECBOS [14] and a CDF detector simulation. As shown in Table II, the acceptance for $W + \geq 1$ jet events increases with E_T^{min} from 24% to 36%. The acceptance for inclusive W events is $(23.9 \pm 0.5)\%$.

Table II also lists the efficiencies for detecting $W \rightarrow e\nu$ events, which include the trigger efficiency, the electron identification (ID) efficiency, and the electron-jet overlap efficiency. The electron-jet overlap efficiency accounts for losses from the electron-jet separation requirement and from jets that overlap electrons in the calorimeter. The electron ID and electron-jet overlap efficiencies are measured from the data using $Z \rightarrow e^+e^-$ events. The combined $W \rightarrow e\nu$ acceptance and detection efficiency is $(19.5 \pm 0.5)\%$ for the inclusive W sample. For the $W + \geq 1$ jet sample, it ranges from $(19 \pm 1)\%$ at $E_T^{min} = 15$ GeV to $(25 \pm 3)\%$ at $E_T^{min} = 95$ GeV.

One of the largest systematic uncertainties on \mathcal{R}_{10} is the jet energy scale uncertainty, which includes calorimeter response and the amount of underlying event energy deposited in the jet cone. Varying the jet energy scale by 1 standard deviation yields a systematic uncertainty on \mathcal{R}_{10} that ranges from 5% at $E_T^{min} = 15$ GeV to 11% at $E_T^{min} = 95$ GeV. Uncertainties in the QCD multijet background result in a 4% to 14% systematic uncertainty on \mathcal{R}_{10} . Other sources of systematic uncertainty on \mathcal{R}_{10} include the $W \rightarrow e\nu$ acceptance, electron-jet overlap effi-

ciency, top quark background, and jet backgrounds from additional interactions and $W\gamma$ production. The overall systematic uncertainty on \mathcal{R}_{10} ranges from 8% at $E_T^{min} = 15$ GeV to 19% at $E_T^{min} = 95$ GeV.

The measured values of \mathcal{R}_{10} for $E_T^{min} = 15$ to 95 GeV are listed in Table III. We compare these measurements to perturbative QCD predictions generated using the DYRAD [15] Monte Carlo program. DYRAD calculates NLO matrix elements for W inclusive (order α_s) and $W + \geq 1$ jet (order α_s^2) production. The cross sections are computed by DYRAD for a particular renormalization scale Q_r and a set of parton distribution functions (PDF) with parton momentum fractions calculated at a factorization scale Q_f . Using the value of Λ_{QCD} associated with the PDF, the strong coupling constant α_s is evolved to the scale Q_r using the second-order expression for the running coupling constant (two-loop α_s).

The theoretical predictions for \mathcal{R}_{10} are found by dividing the DYRAD $W + \geq 1$ jet cross section by the inclusive W cross section for a particular PDF, Q_r , and Q_f . At NLO, the $W + \geq 1$ jet cross section calculation includes diagrams with up to two partons (order α_s^2) in the final state. When two partons have $\Delta R < 0.52$, their 4-vectors are added vectorially to form a jet. This parton clustering simulates the 0.4 cone algorithm used to reconstruct jets in the calorimeter, which can resolve pairs of jets that are separated in ΔR by at least 1.3 times the jet cone size [12]. After jets are smeared in E_T , η , and ϕ to model detector resolution effects [16,17], events that have one or more jets with $E_T > E_T^{min}$ and $|\eta| < 2.4$ are used to calculate the final $W + \geq 1$ jet cross section.

Because jet energies are measured in the data without corrections for energy deposited outside of the jet cone, the measurement of \mathcal{R}_{10} depends on jet cone size. The NLO $W + \geq 1$ jet calculations approximate the shape of jets by producing up to two final-state partons. Therefore, the agreement between data and theory depends on how accurately the theory reproduces the shape of jets.

The measured and predicted values of \mathcal{R}_{10} are compared as a function of E_T^{min} in Figure 1. The NLO QCD predictions for two different PDF sets, MRSA' [18] and CTEQ4M [19], are represented by smooth curves that pass through the calculated values of \mathcal{R}_{10} at each E_T^{min} . The renormalization and factorization scales are set equal to the W boson mass. Data and theory agree well for $E_T^{min} > 25$ GeV. At $E_T^{min} = 0$, the measured value of \mathcal{R}_{10} is unity by definition, whereas the NLO QCD prediction diverges. In addition, soft gluon effects that are not included in the DYRAD calculation may be significant in the low E_T^{min} region. The effect of changing the parton clustering algorithm is small. Varying the ΔR requirement of 0.52 by $\pm 30\%$ yields a change in \mathcal{R}_{10} of less than 10% for all E_T^{min} .

Figure 2 shows a plot of $[\mathcal{R}_{10}(\text{Data}) - \mathcal{R}_{10}(\text{QCD})] / \mathcal{R}_{10}(\text{QCD})$ using MRSA' with $Q_r = Q_f = M_W$. Curves are superimposed for predictions evaluated at two other

scales: $Q_r = Q_f = 0.5 M_W$ and $Q_r = Q_f = 2.0 M_W$. Compared to LO QCD predictions (also generated using DYRAD), the NLO QCD predictions are significantly less sensitive to scale variations; varying Q_r and Q_f together by a factor of two results in a 5% change in \mathcal{R}_{10} at NLO compared to a 15% change at LO. For $Q_r = Q_f = M_W$, the LO and NLO QCD predictions differ by less than 10% over the entire range of E_T^{min} .

A plot of $[\mathcal{R}_{10}(\text{Data}) - \mathcal{R}_{10}(\text{QCD})] / \mathcal{R}_{10}(\text{QCD})$ using CTEQ4M with $Q_r = Q_f = M_W$ is shown in Figure 3. Curves are superimposed for other PDFs in the CTEQ4 family, fit with $\alpha_s(M_Z)$ values ranging from 0.110 to 0.122. The predictions for \mathcal{R}_{10} show very little sensitivity to variations in α_s . Figure 4 shows a plot of \mathcal{R}_{10} vs. $\alpha_s(M_Z)$ for several PDF sets in the MRSA [20] and CTEQ4 families. The measured values of \mathcal{R}_{10} , given for $E_T^{min} = 30$ GeV and $E_T^{min} = 60$ GeV, are represented by horizontal bands. The data and theory are consistent for all values of α_s .

In summary, we have measured the cross section ratio $\mathcal{R}_{10} = \sigma(W + \geq 1 \text{ jet}) / \sigma(W)$ in $W^\pm \rightarrow e^\pm \nu$ events from 108 pb^{-1} of $\bar{p}p$ collisions at $\sqrt{s} = 1.8$ TeV. The cross section ratio is fully corrected for $W \rightarrow e\nu$ backgrounds, acceptances, and efficiencies. Using jets with a cone size of 0.4 in the region $|\eta| < 2.4$, we observe good agreement between data and theory for $E_T^{min} > 25$ GeV, where the predictions lie within 1 standard deviation of the measured values. The small dependence of \mathcal{R}_{10} to variations in α_s , however, precludes an extraction of α_s from this measurement.

We thank the Fermilab staff and the technical staffs of the participating institutions for their vital contributions. We also thank Walter Giele and Nigel Glover for many useful discussions. This work was supported by the U.S. Department of Energy and National Science Foundation; the Italian Istituto Nazionale di Fisica Nucleare; the Ministry of Education, Science and Culture of Japan; the Natural Sciences and Engineering Research Council of Canada; the National Science Council of the Republic of China; the A. P. Sloan Foundation; and the Swiss National Science Foundation.

* Visitor.

- [1] F. Abe *et al.*, Phys. Rev. Lett. **79**, 4760 (1997).
- [2] F. Abe *et al.*, Phys. Rev. Lett. **77**, 448 (1996).
- [3] J. Alitti *et al.*, Phys. Lett. B **263**, 563 (1991).
- [4] M. Lindgren *et al.*, Phys. Rev. D **45**, 3038 (1992).
- [5] S. Abachi *et al.*, Phys. Rev. Lett. **75**, 3226 (1995).
- [6] B. Abbott *et al.*, submitted to the International Europhysics Conference on High Energy Physics, Jerusalem, Israel, 1997 (Report No. FERMILAB-CONF-97-369-E).
- [7] F. Abe *et al.*, Nucl. Instrum. Methods Phys. Res. Sect. A **271**, 387 (1988).
- [8] We use a coordinate system in which z is along the proton direction, ϕ is the azimuthal angle, θ is the polar angle and $\eta \equiv -\ln(\tan \frac{\theta}{2})$ is the pseudorapidity. We take $z = 0$ at the center of the detector for fiducial cuts and at the interaction point for event variables.
- [9] An isolated electron is one for which the calorimeter E_T in a cone of radius 0.4 in η - ϕ around the electron cluster is less than 10% of the electron E_T .
- [10] F. Abe *et al.*, Phys. Rev. D **44**, 29 (1991); our selection is the same as in this reference except for (i) $0.5 < E/(pc) < 2.0$ and (ii) $\chi_{strip}^2 < 10$.
- [11] F. Abe *et al.*, Phys. Rev. D **52**, 2624 (1995).
- [12] F. Abe *et al.*, Phys. Rev. D **45**, 1448 (1992).
- [13] F. Abe *et al.*, Phys. Rev. D **47**, 4857 (1993).
- [14] F.A. Berends, W.T. Giele, H. Kuijf, and B. Tausk, Nucl. Phys. **B357**, 32 (1991).
- [15] W.T. Giele, E.W.N. Glover, and D.A. Kosower, Nucl. Phys. **B403**, 633 (1993).
- [16] F. Abe *et al.*, Phys. Rev. D **57**, 67 (1998), with minor modifications for 0.4 jet cones.
- [17] J.R. Dittmann, Ph.D. thesis, Duke University, 1998.
- [18] A.D. Martin, R.G. Roberts, W.J. Stirling, Phys. Lett. B **354**, 155 (1995).
- [19] H.L. Lai *et al.*, Phys. Rev. D **55**, 1280 (1997).
- [20] A.D. Martin, R.G. Roberts, W.J. Stirling, Phys. Lett. B **356**, 89 (1995).

TABLE I. Backgrounds (%) in the $W + \geq 1$ jet sample.

	E_T^{min} (GeV)		
	15	55	95
QCD multijet	13 ± 4	14 ± 5	28 ± 13
$W \rightarrow \tau\nu$	2.9 ± 0.3	7.8 ± 1.2	6.4 ± 2.4
$Z \rightarrow e^+e^-$	1.8 ± 0.1	2.3 ± 0.2	2.2 ± 0.4
$Z \rightarrow \tau^+\tau^-$	0.6 ± 0.1	1.8 ± 0.1	1.8 ± 0.3
Top	0.5 ± 0.1	3.1 ± 0.6	5.1 ± 1.0
X -jet, $W\gamma$	3.6 ± 3.6	0.3 ± 0.3	0.3 ± 0.3

 TABLE II. $W^\pm \rightarrow e^\pm\nu$ acceptance and efficiencies (in %) for the $W + \geq 1$ jet sample.

	E_T^{min} (GeV)		
	15	55	95
Acceptance	24 ± 1	29 ± 1	36 ± 2
Trigger	95 ± 1	94 ± 2	93 ± 2
Electron ID	88 ± 1	84 ± 5	77 ± 13
Electron-jet overlap	94 ± 1	95 ± 1	96 ± 3

 TABLE III. Measured values of $\mathcal{R}_{10} = \sigma(W + \geq 1 \text{ jet}) / \sigma(W)$ for E_T^{min} ranging from 15 to 95 GeV, compared to QCD predictions using MRSA' with $Q_r = Q_f = M_W$. The uncertainties on $\mathcal{R}_{10}(\text{Data})$ are statistical and systematic, respectively.

E_T^{min} (GeV)	$\mathcal{R}_{10}(\text{Data})$	$\mathcal{R}_{10}(\text{QCD})$
15	$0.1301 \pm 0.0057 \pm 0.0102$	0.1557
20	$0.0868 \pm 0.0043 \pm 0.0070$	0.1036
25	$0.0649 \pm 0.0035 \pm 0.0053$	0.0718
30	$0.0484 \pm 0.0028 \pm 0.0039$	0.0515
35	$0.0363 \pm 0.0023 \pm 0.0029$	0.0377
40	$0.0275 \pm 0.0019 \pm 0.0025$	0.0284
45	$0.0215 \pm 0.0017 \pm 0.0019$	0.0217
50	$0.0161 \pm 0.0014 \pm 0.0015$	0.0166
55	$0.0126 \pm 0.0012 \pm 0.0012$	0.0129
60	$0.0097 \pm 0.0011 \pm 0.0011$	0.0102
65	$0.0072 \pm 0.0009 \pm 0.0009$	0.0080
70	$0.0054 \pm 0.0007 \pm 0.0007$	0.0063
75	$0.0044 \pm 0.0007 \pm 0.0006$	0.0051
80	$0.0037 \pm 0.0006 \pm 0.0006$	0.0041
85	$0.0028 \pm 0.0006 \pm 0.0004$	0.0033
90	$0.0025 \pm 0.0006 \pm 0.0004$	0.0027
95	$0.0019 \pm 0.0005 \pm 0.0004$	0.0022

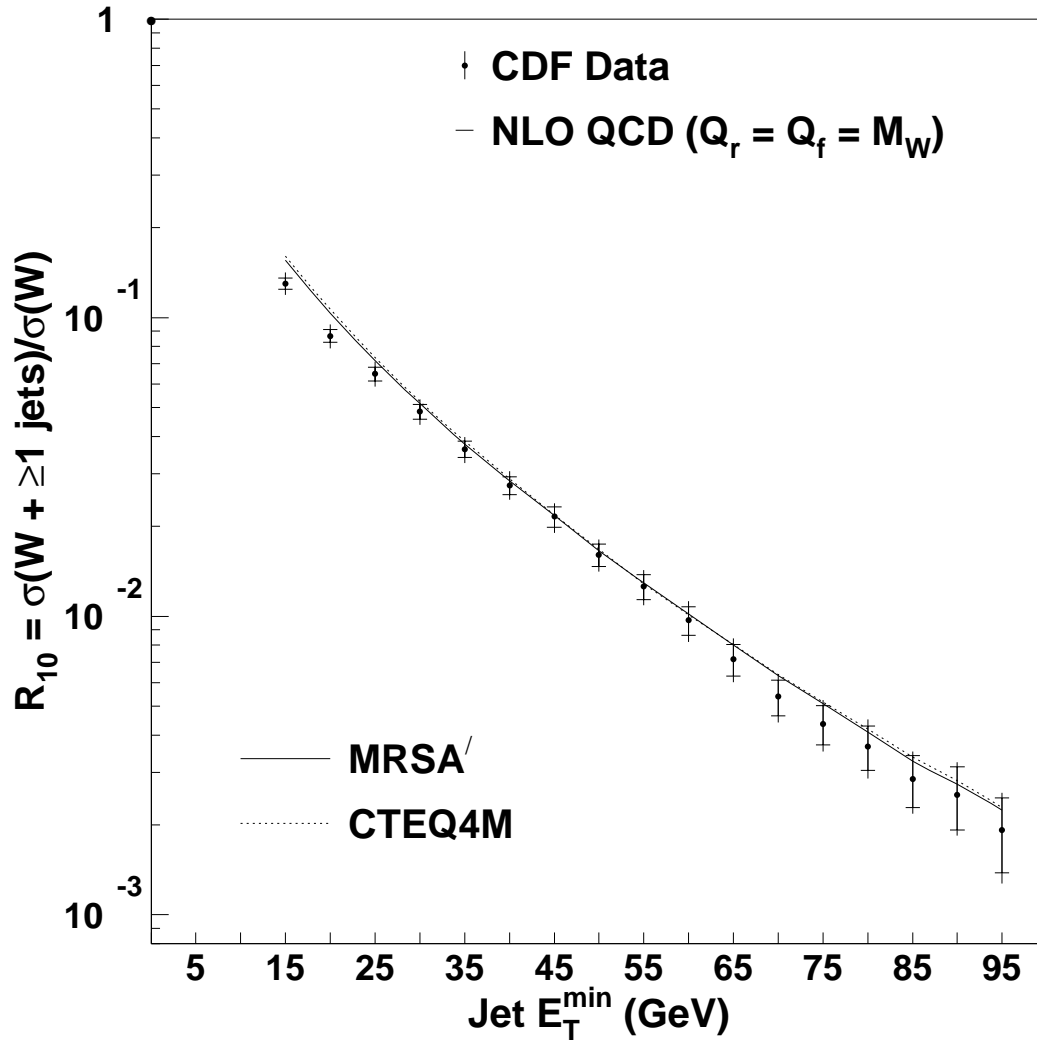


FIG. 1. R_{10} measurement vs. jet E_T^{\min} , compared to NLO QCD predictions calculated using the MRSA' and CTEQ4M parton distribution functions. The renormalization and factorization scales are set equal to the W boson mass. The inner error bars include statistical uncertainties only; the outer error bars include both statistical and systematic uncertainties.

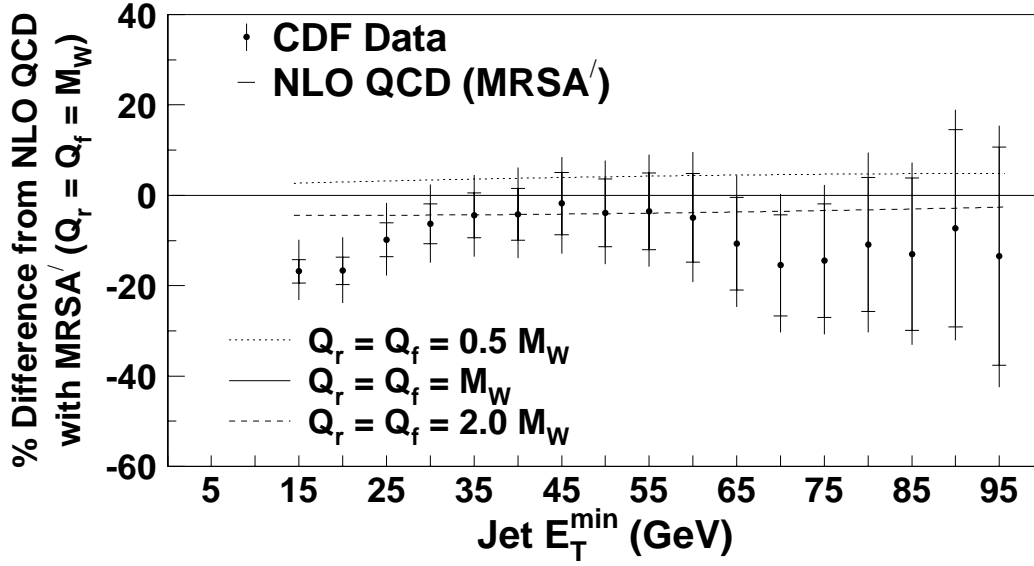


FIG. 2. Ratio of $\mathcal{R}_{10}(\text{Data}) - \mathcal{R}_{10}(\text{QCD})$ to $\mathcal{R}_{10}(\text{QCD})$ for MRSA' using $Q_r = Q_f = M_W$ (points). The superimposed curves show the sensitivity of the NLO QCD prediction to the renormalization and factorization scales, which are set to 0.5 and 2.0 times the W boson mass.

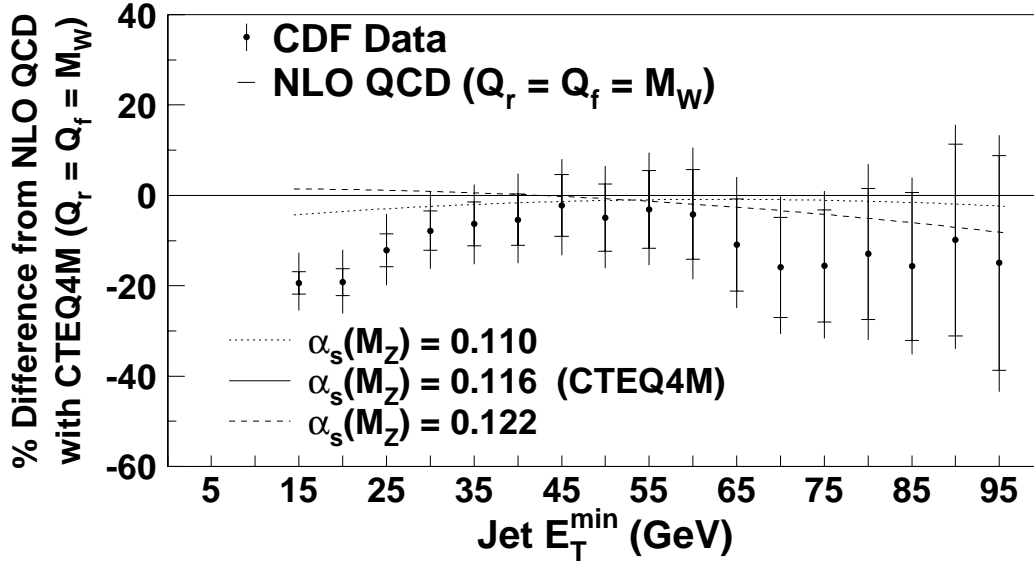


FIG. 3. Ratio of $\mathcal{R}_{10}(\text{Data}) - \mathcal{R}_{10}(\text{QCD})$ to $\mathcal{R}_{10}(\text{QCD})$ for CTEQ4M using $Q_r = Q_f = M_W$ (points). Curves are superimposed for other PDFs in the CTEQ4 family with $\alpha_s(M_Z)$ values ranging from 0.110 to 0.122.

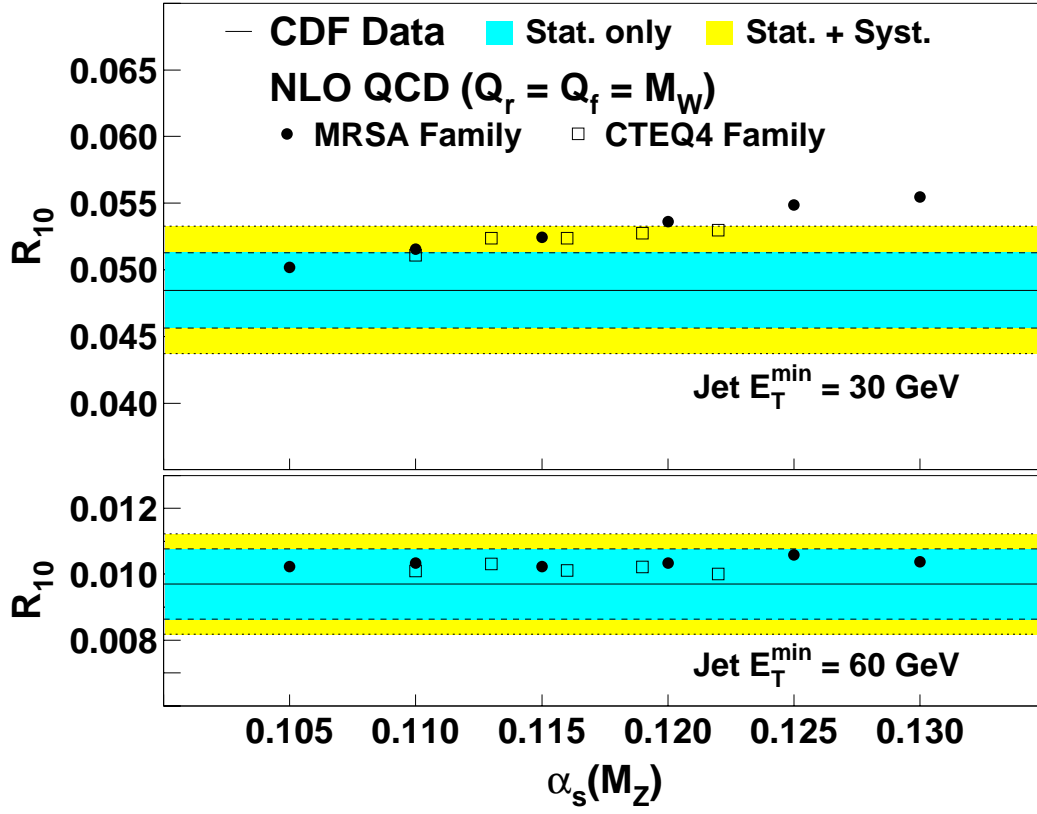


FIG. 4. \mathcal{R}_{10} vs. $\alpha_s(M_Z)$ for PDFs in the MRSA and CTEQ4 families. The symbols represent the predicted values of \mathcal{R}_{10} at $E_T^{\min} = 30$ GeV (top) and $E_T^{\min} = 60$ GeV (bottom), compared to the measured values (shaded bands).